Book Chapter

Evaluation and Improvement of Backup Capacity for Household Electric Vehicle Uninterruptible Power Supply (EV-UPS) Systems

Wenping Zhang[1,2]

[1]Department of Electrical and Information Engineering, Tianjin University, Tianjin 300072, China
[2]Research Center, Ginlong Technologies Co., Ltd., Ningbo 315712, China

***Corresponding Author: Wenping Zhang,** Department of Electrical and Information Engineering, Tianjin University, Tianjin 300072, China

Published **November 26, 2024**

This Book Chapter is a republication of an article published by Wenping Zhang, et al. at Energies in June 2023. (Zhang, W.; Wang, Y.; Xu, P.; Li, D.; Liu, B. Evaluation and Improvement of Backup Capacity for Household Electric Vehicle Uninterruptible Power Supply (EV-UPS) Systems. Energies 2023, 16, 4567. https://doi.org/10.3390/en16124567)

How to cite this book chapter: Wenping Zhang. Evaluation and Improvement of Backup Capacity for Household Electric Vehicle Uninterruptible Power Supply (EV-UPS) Systems. Top 10 Contributions in Energy Research. Hyderabad, India: Academic Reads. 2024.

Acknowledgement: The authors would like to thank the University of New Brunswick for their assistance with this project.

Abstract

The use of electric vehicles (EVs) for household Uninterruptible Power Supplies (UPSs), particularly in rural areas, can greatly improve household power reliability. However, because EVs are mobile, the evaluation of backup capacity for EV-UPS systems is completely different when compared to traditional UPSs. As a result, the focus of this paper is on the evaluation and improvement of backup capacity for EV-UPS systems. The architectures for EV-UPS systems are presented first. The methodology for calculating backup capacity for EV-UPS systems is then presented, followed by four detailed cases based on different grid failure times. Furthermore, the impact of system operating parameters on backup capacity, such as different load power, EV mobility pattern parameters, and grid outage durations, is investigated. The results of backup capacity in cases of different operating parameters are detailed using an EV mobility model. An improved strategy for increasing backup capacity is proposed, in which more backup energy can be released during a power outage. Meanwhile, the next trip requirement is unaffected. The backup capacity with the improved strategy is then calculated and compared to the results with the traditional strategy. Finally, a 5kW EV-UPS experimental platform is constructed, and the experimental results are presented to validate the proposed method.

Keywords

EV; UPS; Backup Capacity; Power Outage; Reliability

1. Introduction

Greenhouse gas emissions and global warming are currently posing a serious threat to our environment. It is widely acknowledged that using electricity instead of gasoline to power

transportation can significantly reduce greenhouse gas emissions and combat climate change [1]. As a result, the development of electric vehicles is becoming a global trend. Furthermore, EVs with bidirectional capabilities can serve multiple functions in smart power systems [2]. Bidirectional EV systems are currently available in three configurations: vehicle to home (V2H), vehicle to vehicle (V2V), and vehicle to grid (V2G) [3].

Power flows between EVs and homes in V2H applications. The system configuration is relatively simple and straightforward in practice. In [4,] EVs are used as energy storage to smooth household loads in V2H applications, particularly when renewables are used. In addition, to optimize home power consumption with EVs, an optimal centralized scheduling is proposed [5]. Furthermore, Nissan proposed the scenario of building smart homes using "LEAF to Home" systems. [6] extends bidirectional EV systems to function as UPSs to improve household power reliability. It is well known that current household power is not as reliable as expected, particularly in remote areas. Using British Columbia as an example, the average number of power outages in the province is two per year, with each outage lasting an average of three hours [7]. Furthermore, in rural areas, these figures are even worse. In Valemount, British Columbia, for example, power outages occur eight times per year and last an average of 4.5 hours. As a result, by using EVs as UPSs for households, particularly in rural areas, the reliability of household power can be greatly improved. Furthermore, when EVs are parked at home, the stored energy can be fully utilized in EV-UPS systems. EVs also have a much faster response time and lower operating costs when compared to home backup generators [8]. As a result of these benefits, EV-UPS systems gain a lot of attention from researchers and industries.

Traditionally, UPS architectures are classified into three types: on-line, off-line, and line-interactive [9]. Among the three configurations, the off-line structure is suitable for household EV-UPS systems due to its simple design, low cost, and high density. As a result, offline EV-UPS system architectures are investigated, and numerous on-board and off-board bidirectional topologies are proposed. The two-stage architecture, consisting

of a front-end ac/dc followed by an isolated dc/dc, is typically chosen for on-board bidirectional converters [10]. Interleaved boost, bridgeless/dual boost, and bridgeless interleaved boost are some of the popular front-end ac/dc converters [10]. The typical topologies for isolated dc/dc converters include full-bridge LLC resonant converters, interleaved ZVS FB converters with voltage doublers, and zero-voltage switching (ZVS) FB converters with capacitive output filters [10,11].

Another area of study for researchers is the operating modes and transition between different modes for offline EV-UPS systems. [6] details two cases for the transition to backup mode, which include the EV only plugged in at home and the EV plugged in and also charging. The results, however, are only verified with linear loads, which is deemed unrealistic. As a result, [12] includes a more detailed analysis and experimental validation for nonlinear electrical appliances. A fast grid failure detection with bi-directional converters is critical during the transition. [12] examines and compares two grid failure detection algorithms: rms voltage calculation for half-cycle grid and rms voltage estimation using a Kalman filter. A sliding window rms calculation is typically used for grid failure detection in order to reduce detection time [13].

The significant difference between EV-UPS systems and traditional UPSs is that the EV battery is mobile, and the system can only backup the grid when the EV is plugged in [8]. Furthermore, when the grid fails, the EV battery is not always full, and the stored energy is dependent on the EV mobility pattern and charging scheduling. As a result, the backup capacity of EV-UPS systems differs significantly from that of traditional UPSs. However, there have been few papers that discuss how to evaluate backup capacity for EV-UPS systems. There are two important criteria for evaluating backup capacity in UPS systems: 1) the backup energy that UPSs can provide, and 2) the backup time that UPSs can cover [13]. These two criteria are closely related in EV-UPS systems to the EV mobility pattern and charging scheduling. It is difficult to precisely model driving habits and battery state of charge (SOC) for EV mobility. Most existing studies predict EV availability using historical data and model EV behavior as an arrival and departure process. The

Gaussian distribution, Poisson process, and Markov chain [14] are used to model the arrival and departure time. Furthermore, the EVs have varying SOCs, which are also modelled as normal or lognormal distributions. Numerous strategies for EV charging scheduling have been proposed, which basically fall into three categories [15]. The first category is from the perspective of the grid, and the optimization goals include minimizing power variances, minimizing power losses, and maximizing grid reliability. The second category is from the perspective of users, and the optimization objectives include minimizing charging costs, increasing EV average SOCs, increasing user convenience, and so on [16]. Furthermore, a few papers [15] jointly optimize the benefits of both grid-side and EV-side benefits. A variety of smart charging/discharging algorithms, such as convex optimization, linear programming, game theory, swarm particle optimization, and heuristic methods, are proposed to implement these functions. [17] proposes a methodology for managing smart home appliances alongside EVs, taking into account demand rebound and consumer convenience indices, in order to reduce network stress, congestion, and demand rebound. [18] develops a model to forecast maximum demand based on the increasing penetration of EV consumers. [19] proposes a frequency regulation strategy with support for electric vehicles based on a novel fuzzy-based dual-stage controller and a modified dragonfly algorithm.

In general, no papers have been reported to develop strategies to improve backup performance for EV-UPS systems. As a result, the purpose of this paper is to evaluate and improve the backup capacity of household EV-UPS systems. The main contributions of this paper are listed below.

1) Based on the EV mobility pattern, a methodology for calculating backup capacity for EV-UPS systems is proposed.
2) The effect of system operating parameters on backup capacity for EV-UPS systems is thoroughly examined. Load power, EV mobility pattern parameters, and grid outage duration are among the operating parameters.
3) An improved strategy is proposed to maximize backup capacity while maintaining the need for next-day trips.

2. EV-UPS Architecture

2.1 Singular-EV UPS Architecture

Figure 1(a) depicts the original household architecture, with the load supplied by the grid. Refrigerators, air conditioners, lights, cooking stoves, washers and dryers, and other major appliances are included. If there is only one EV, the simplest architecture for the EV-UPS system is shown in Figure 1(b), which includes a bi-dc/ac converter.

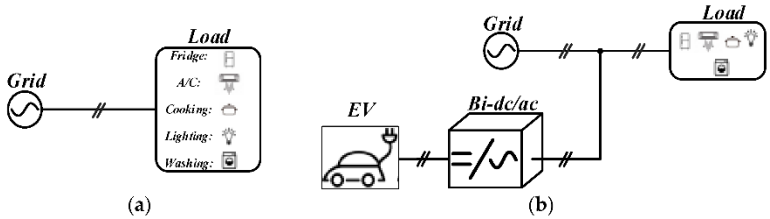

Figure 1: Singular-EV UPS architecture (a) Original household architecture; (b) Singular-EV UPS Architecture.

The EV-UPS system has three operating modes, as illustrated in Figure 2. The EV-UPS system differs significantly from traditional UPS systems in that it is mobile. The EV cannot charge or discharge itself when it is traveling and not at home (see Figure 2(a)). When the EV is plugged in and the grid is normal, it can be charged using the bi-dc/ac converter, as illustrated in Figure 2(b). In the event that the grid fails, the EV discharges power to supply the load, as shown in Figure 2(c).

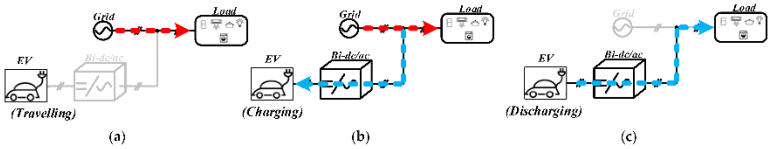

Figure 2: Three operating modes (a) EV not at home; (b) EV charging; (c) EV discharging when the grid fails.

2.2 Multiple-EV UPS Architecture

The number of EVs in a large household or apartment complex is usually greater than one. Figure 3 depicts two different types of multiple-EV UPS architectures. To achieve modular design, all EV connections to the grid or to the load must be the same.

There are no dc-buses in this architecture, and each EV is connected to the grid via a bi-dc/ac converter, as shown in Figure 3(a). A dc-bus is added in Figure 3(b), and each EV is connected to it via a bi-dc/dc converter. The dc-bus is then linked to the grid via a dc/ac inverter. However, the dc/ac inverter's reliability is critical. If the dc/ac inverter fails, neither EV will be able to charge or discharge.

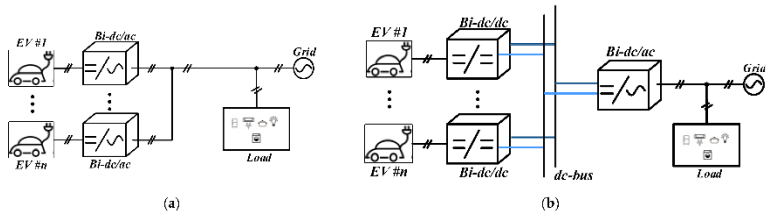

Figure 3: Multiple-EV UPS architectures (a) Architecture 1; (b) Architecture 2.

The sections that follow will concentrate on EV-UPS backup capacity evaluation. The calculation will be demonstrated using a single household EV UPS system, but the concept can also be applied to multiple-EV UPS systems.

3. Backup Capacity Calculation

The most important backup criteria in UPS systems are 1) the backup energy that UPSs can provide and 2) the backup time that UPSs can cover. The evaluation of these two criteria for EV-UPS systems, however, differs because the EV-UPS systems have different features.

1) The EV-UPS system's battery is mobile, and the system can only support the grid when the EV is plugged in.
2) When the grid fails, the EV battery is not always full, and the stored energy is dependent on the EV mobility pattern and charging scheduling.

Using a single household EV system as an example, Figure 4 depicts a typical EV mobility pattern in which the EV is only connected to the grid during home charging (after t_{HA} and before t_{HD}). The following will calculate the backup energy and backup

time that the EV-UPS system can provide based on the EV mobility pattern.

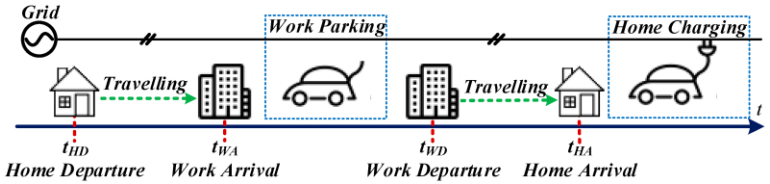

Figure 4: EV daily mobility pattern.

The backup energy E_{BU} and backup time T_{BU} that the EV-UPS can provide vary depending on the grid failure time. Figure 5 depicts four cases based on different grid failure time t_f. The duration of the grid's outage is assumed here as T_D.

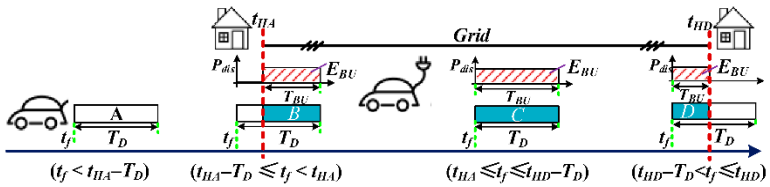

Figure 5: Four cases for backup capacity calculation.

3.1 Case A ($t_f < t_{HA}-T_D$)

In case A, the EV is disconnected from the grid for the duration of T_D after the grid fails. As a result, the EV battery's stored energy cannot be discharged to the grid. Both the backup energy E_{BU} and backup time T_{BU} are zero.

$$\begin{cases} E_{BU}(t_f) = 0 \\ T_{BU}(t_f) = 0 \end{cases} \quad (Case\ A) \tag{1}$$

3.2 Case C ($t_{HA} \leq t_f \leq t_{HD}-T_D$)

Cases B and D are special cases of Case C, which is examined first. Five parameters are first defined in Figure 6 to describe various situations in Case C. Figure 6 shows the charging time t_{chg} which is from the energy $E(t_f)$ to the fully charged EV. t_{dis} is

the time required to discharge the energy $E(t_f)$ to the allowed minimum energy E_{min}. The EV charging time from the minimum charge to the full charge is represented by t_{chg_emp}. If the energy $E(t_f)$ can withstand a continuous discharging of T_D, the charging time to fully charge the EV after this discharging is t_{chg_Td}. The remaining time to t_{HD} after T_D is denoted by t_{left}. It is worth noting that the discharging rate is not constant in practice, and changes in real-time.

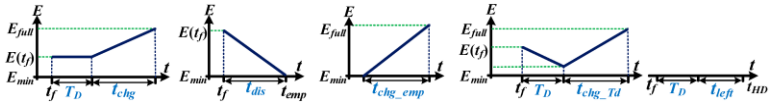

Figure 6: Symbol description for case C.

The values of the five above parameters are calculated for various grid failing time t_f. Then, using the relationship between these five parameters, five sub-cases for case C are obtained, as shown in Figure 7.

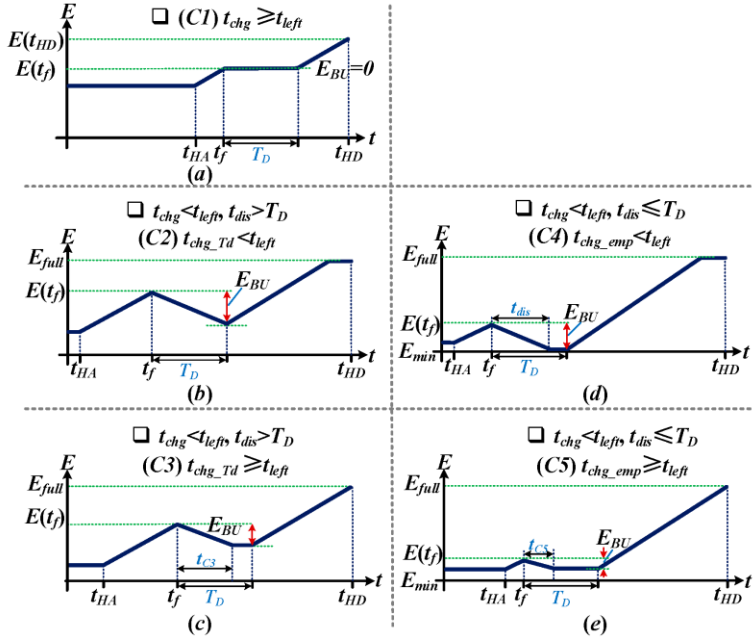

Figure 7: Five sub-cases for case C.

Here, two assumptions are made.

1) The EV battery should be fully charged before departure to ensure the daily trip requirement. This strategy is commonly used in practice and is known as the full charge before departure (FCBD) strategy in this context.
2) During the power outage, the EV cannot be charged.

In the case of C1, t_{chg} is greater than t_{left}. This means that the EV cannot discharge energy during the power outage period T_D in order to seek full charge before departure. As a result, as shown in (2), the backup energy E_{BU} is zero in this case. In contrast, t_{chg} is less than t_{left} in other cases (C2~C5). This means that in cases C2~C5, the EV can discharge energy during T_D.

$$\begin{cases} E_{BU}(t_f) = 0 \\ T_{BU}(t_f) = 0 \end{cases} \quad (Case\ C1) \tag{2}$$

In cases C2 and C3, t_{dis} is greater than T_D, indicating that the EV has enough energy to discharge for a period of T_D. In the case of C2, t_{chg_Td} is less than t_{left}, indicating that there is still enough time for the EV to be fully charged before departure after discharging for the duration of T_D. As a result, the EV can discharge continuously throughout the T_D. In the case of C2, the backup energy E_{BU} and backup time T_{BU} are expressed as shown in (3).

$$\begin{cases} E_{BU}(t_f) = \int_{t_f}^{t_f+T_D} P_{dis}(t)dt = \int_{t_f}^{t_f+T_D} \frac{P_L(t)}{\eta_{dis}}dt \\ T_{BU}(t_f) = T_D \end{cases} \quad (Case\ C2) \tag{3}$$

where P_{dis} is the discharging power of the EV battery, P_L is the load power, and η_{dis} is the discharging efficiency.

In case *C3*, t_{chg_Td} is greater than t_{left}, this means that if the discharging lasts the duration of T_D, the EV battery will not be fully charged before departure. As a result, the EV is only

permitted to discharge for a portion of the T_D. Figure 7(c) shows the backup energy E_{BU} and backup time T_{BU} in case C3 in (4).

$$\begin{cases} E_{BU}(t_f) = P_{chg} t_{left} - \left(E_{full} - E(t_f)\right) \\ \int_{t_f}^{t_f + t_{C3}} \frac{P_L(t)}{\eta_{dis}} dt = E_{BU}(t_f) \qquad (Case\ C3) \\ T_{BU}(t_f) = t_{C3} \end{cases} \quad (4)$$

where P_{chg} is the EV charging power.

In cases C4 and C5, t_{dis} is less than T_D, implying that the energy stored in the EV can be fully discharged during T_D. In case C4, t_{chg_emp} is less than t_{left}, indicating that there is sufficient time for the EV battery to be fully charged after being fully discharged during T_D. As a result, the stored energy can be fully released. The associated backup energy E_{BU} and backup time T_{BU} are shown in (5).

$$\begin{cases} E_{BU}(t_f) = E(t_f) - E_{min} \\ T_{BU}(t_f) = t_{dis} \end{cases} \quad (Case\ C4) \qquad (5)$$

where E_{min} is the allowed minimum energy, which is normally set by EV manufacturers.

In case *C5*, t_{chg_emp} is greater than t_{left}, this indicates that there is insufficient time for the EV battery to be fully charged after being fully discharged during T_D. As a result, the EV is only permitted to discharge a portion of the stored energy. The backup energy E_{BU} and backup time T_{BU} for case C5 are shown in (6) based on Figure 7(e).

$$\begin{cases} E_{BU}(t_f) = P_{chg} t_{left} - \left(E_{full} - E(t_f)\right) \\ \int_{t_f}^{t_f + t_{C5}} \frac{P_L(t)}{\eta_{dis}} dt = E_{BU}(t_f) \qquad (Case\ C5) \\ T_{BU}(t_f) = t_{C5} \end{cases} \quad (6)$$

The expression of E_{BU} for case C is shown in (7) by combining (1)-(6). Similarly, the T_{BU} expression for case C can be obtained.

$$E_{BU}(t_f) = \begin{cases} 0 & (C1) \\ \int_{t_f}^{t_f+T_D} \frac{P_L(t)}{\eta_{dis}} dt & (C2) \\ E(t_f) - E_{min} & (C4) \\ P_{chg} t_{left} - \left(E_{full} - E(t_f)\right) & (C3, C5) \end{cases} \quad (7)$$

3.3 Case B ($t_{HA} - T_D \le t_f < t_{HA}$)

Case B is a subset of Case C. As shown in Figure 5, the EV in Case B is not connected to the grid until the time of t_{HA}, which is unlikely in Case C. As a result, the starting time for providing backup power in case B is t_{HA} rather than t_f. Using the same method as in Case C, redefine the parameters in Figure 6, as shown in Figure 8.

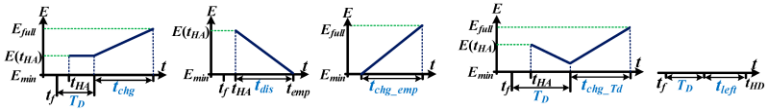

Figure 8: Symbol description for Case B.

Recalculate these five parameters to get five sub-cases for case B. (8) expresses the corresponding expression for E_{BU} in case B. The expression for T_{BU} can be obtained in the same way.

$$E_{BU}(t_f) = \begin{cases} 0 & (B1) \\ \int_{t_{HA}}^{t_f+T_D} \frac{P_L(t)}{\eta_{dis}} dt & (B2) \\ E(t_{HA}) - E_{min} & (B4) \\ P_{chg} t_{left} - \left(E_{full} - E(t_{HA})\right) & (B3, B5) \end{cases} \quad (8)$$

3.4 Case D ($t_{HD}-T_D < t_f \leq t_{HD}$)

Case D is also a subset of Case C. The duration from the grid failure to the EV departure is less than T_D in this case, as shown in Figure 5, indicating that the power outage lasts until the EV departure. In order to fully charge before departure, the EV cannot discharge backup energy (see Figure 9). As a result, as shown in (9), E_{BU} and T_{BU} are both zero.

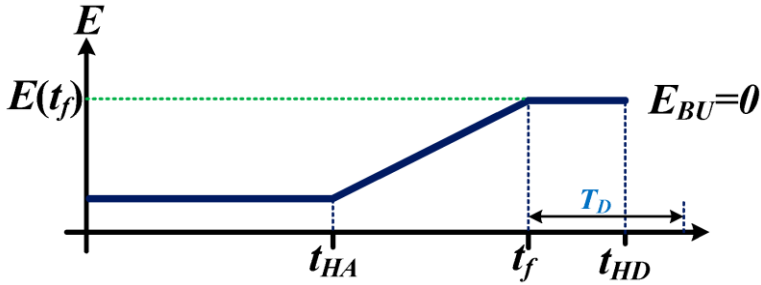

Figure 9: Case D.

$$\begin{cases} E_{BU}(t_f) = 0 \\ T_{BU}(t_f) = 0 \end{cases} \quad (Case\ D) \tag{9}$$

As a result, the backup energy E_{BU} and backup time T_{BU} can be calculated for various scenarios. Another criterion, the load downtime percentage χ_{DT}, is also introduced here. The load downtime percentage over the grid outage duration can be calculated using the backup time T_{BU}, as described in (10). The downtime percentage of the load χ_{DT} can be reduced by increasing the backup time T_{BU} from (10). The downtime percentage can also indicate load reliability.

$$\chi_{DT}(t_f) = (1 - \frac{T_{BU}(t_f)}{T_D}) \times 100\% \tag{10}$$

4. Impact of System Parameters on Backup Capacity

Based on the previous section, the following section will present case studies and calculate the backup energy and backup time, as well as the load downtime percentages, for various grid failure times. As mentioned in the previous section, these backup performance criteria (E_{BU}, T_{BU} and χ_{DT}) are closely related to a number of system operating parameters: 1) load power P_L, 2) EV travel pattern parameters (e.g., t_{HD}, t_{HA}, and $E(t_{HA})$), and 3) grid outage duration T_D. As a result, the impact of these parameters will be examined as well. The following is the methodology used in this case. To begin, obtain system parameters such as charging power P_{chg}, discharging power P_{dis}, travel distance L, home departure time t_{HD}, home arrival time t_{HA}, power outage duration T_D, and so on. Then, determine which case with these parameters is located, and the detailed analysis is in section 2. The backup energy E_{BU} and backup time T_{BU} can then be calculated using the equations in section 2 for various cases. Finally, with (10), the load downtime percentage χ_{DT} is calculated.

4.1. Constant Maximum Load

To begin, the load is assumed to be constant. Table 1 shows the parameters for the case study assuming that the load is the maximum power of the EV-UPS system.

Table 1: System parameters.

Item	*Parameter*	*Item*	*Parameter*
Electric vehicle	*Nissan Leaf*	Charging power P_{chg}	*6.6kW*
Discharging power P_{dis}	*6.6kW*	Travel distance L	*25mile*
Home departure time t_{HD}	*8:00h*	Home arrival time t_{HA}	*18:00h*
EV full energy E_{full}	*40kWh*	EV minimum energy E_{min}	*0.2×40kWh*
Power outage duration T_D	*1hour*	Efficiency η_{dis}	*0.95*
Household load P_L	*6.6kW× η_{dis}*	Number of EV per household	*1*

Given an EV battery energy consumption rate of 40kWh per 150 miles, the EV remaining energy when returning home is shown in (11).

$$E(t_{HA}) = (1 - \frac{L}{150}) \times E_{full} \tag{11}$$

where L is the travelling distance.

Obtain the system parameters at the time of the grid failure for various grid failure time. Then, figure out which case the system is in and plug the parameters into the corresponding expression to get the backup energy (E_{BU}) and backup time (T_{BU}).

The case study results are shown in Figure 10 based on Table 1 and the analysis in Section 2. According to Figure 10(a), the EV-UPS is often used in case C, where the backup energy can reach up to 6.6kWh, when the grid fails during the home charging time (after t_{HA} and before t_{HD}). The associated backup time can reach an hour according to Figure 10(b). As a result, the EV-UPS can completely cover the grid loss and reduce the load downtime to zero, as shown in Figure 10(c). Additionally, Figure 10(a) shows that the EV-UPS is primarily in case A when the grid fails during non-charging time, and the backup energy and backup time are both zero. Therefore, as illustrated in Figure 10(c), the load downtime percentage can reach 100%.

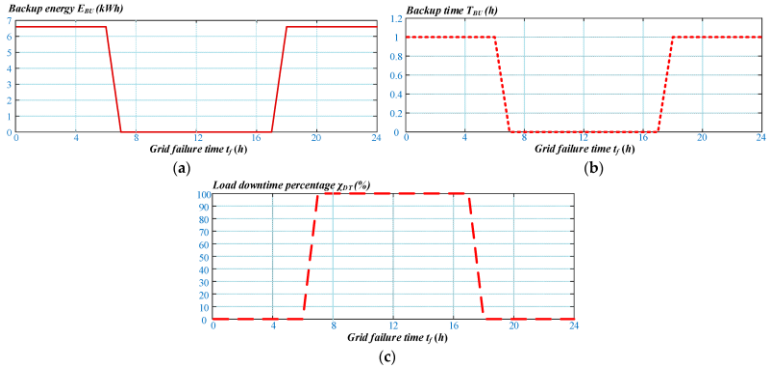

Figure 10: Results of E_{BU}, T_{BU} and χ_{DT} for the case study (a) Backup energy E_{BU}; (b) Backup time T_{BU}; (c) Load downtime percentage χ_{DT}.

4.1.1 Uncertainty of Daily Travelling Parameters

The EV traveling parameters (e.g., t_{HD}, t_{HA}, and $E(t_{HA})$) are fixed in the preceding case study. A Monte Carlo simulation is performed to account for the uncertainty of the daily travel parameters. The average daily trip distance is assumed to be a log-normal distribution with a standard deviation of 0.5. (12) depicts the relevant probability density distribution.

$$f_D(L) = \frac{1}{\sqrt{2\pi}\sigma_D L} e^{\left[-\frac{(lnL-\mu_D)^2}{2\sigma_D^2}\right]} \tag{12}$$

where μ_D= 3.22 and σ_D= 0.5.

The EV home arrival time and home departure time are assumed to be normal distributions, and the related probability density functions are illustrated in (13)-(14), where σ_{HA} is 3.4 and σ_{HD} is 3.24.

$$f_{HA}(t_{HA}) = \begin{cases} \frac{1}{\sqrt{2\pi}\sigma_{HA}} e^{\left[-\frac{(t_{HA}-\mu_{HA})^2}{2\sigma_{HA}^2}\right]}, \mu_{HA} - 12 < t_{HA} \le 24 \\ \frac{1}{\sqrt{2\pi}\sigma_{HA}} e^{\left[-\frac{(t_{HA}+24-\mu_{HA})^2}{2\sigma_{HA}^2}\right]}, 0 < t_{HA} \le \mu_{HA} - 12 \end{cases} \tag{13}$$

$$f_{HD}(t_{HD}) = \begin{cases} \frac{1}{\sqrt{2\pi}\sigma_{HD}} e^{\left[-\frac{(t_{HD}-\mu_{HD})^2}{2\sigma_{HD}^2}\right]}, 0 < t_{HD} \le 12 + \mu_{\mathrm{HD}} \\ \frac{1}{\sqrt{2\pi}\sigma_{HD}} e^{\left[-\frac{(t_{HD}-24-\mu_{HD})^2}{2\sigma_{HD}^2}\right]}, 12 + \mu_{\mathrm{HD}} < t_{HD} \le 24 \end{cases} \tag{14}$$

where μ_{HA}= 18, μ_{HD} = 8, σ_{HA} = 3.4, and σ_{HD}= 3.24.

The probability density functions, including f_D, f_{HA} and f_{HD}, are plotted as shown in Figure 11.

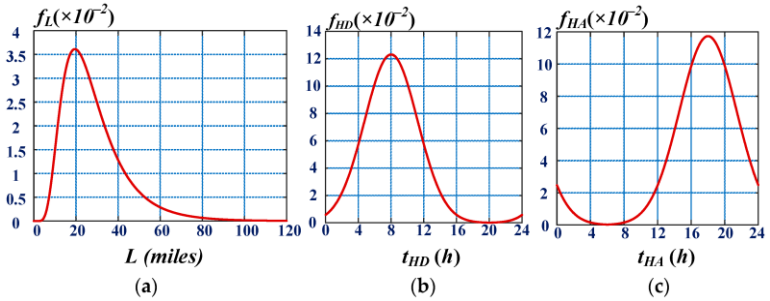

Figure 11: Probability density functions (a) f_L; (b) f_{HD}; (c) f_{HA}.

The Monte Carlo simulation is run for 10,000 times. The expected backup energy ($\overline{E_{BU}}$), expected backup time ($\overline{T_{BU}}$), and expected load downtime percentage ($\overline{\chi_{DT}}$) for these ten thousand tests can then be computed using (15).

$$\begin{cases} \overline{E_{BU}}(t_f) = \dfrac{1}{N}\sum_{i=1}^{10000} E_{BU}(t_f, i) \\ \overline{T_{BU}}(t_f) = \dfrac{1}{N}\sum_{i=1}^{10000} T_{BU}(t_f, i) \\ \overline{\chi_{DT}}(t_f) = (1 - \dfrac{\overline{T_{BU}}(t_f)}{T_D}) \times 100\% \end{cases} \tag{15}$$

where $E_{BU}(t_f, i)$ and $T_{BU}(t_f, i)$ are the backup energy and time for the i^{th} time of the Monte Carlo simulation, respectively; N denotes the number of tests.

Figure 12 shows the findings of $\overline{T_{BU}}$ and $\overline{\chi_{DT}}$ for the case study. According to Figure 12, when the grid fails during the day, the backup period that the EV-UPS can provide is quite short, resulting in a higher proportion of load downtime. The main reason for this is that the likelihood of the EV being connected to the grid is low throughout the day. When the grid fails during the night, the probability of EVs connected to the grid is greater, resulting in longer backup time and a lower percentage of load downtime. The proportion of load outage can be brought below 20%, particularly if the grid breakdown happens between 0:00

and 4:00. Thus, the EV-UPS system can significantly improve load dependability.

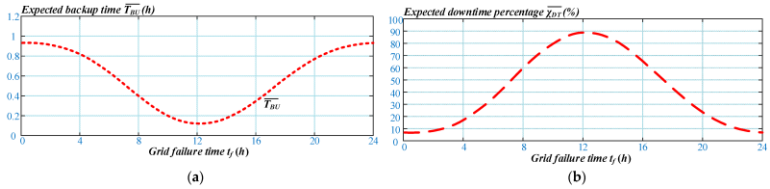

Figure 12: Results of $\overline{\mathrm{T_{BU}}}$ and $\overline{\chi_{\mathrm{DT}}}$ for the Monte Carlo simulation (a) Expected backup time $\overline{\mathrm{T_{BU}}}$; (b) Expected load downtime percentage $\overline{\chi_{\mathrm{DT}}}$.

4.1.2 Different grid outage duration $\mathrm{T_D}$

In the analysis above, the grid outage length T_D is fixed as one hour. Figure 13 shows the outcomes using the same methodology for various grid outage lengths. According to Figure 13(a), the backup time ($\overline{T_{BU}}$) normally increases as the grid outage length increases. In contrast, if T_D exceeds 5 hours and the grid failure occurs at night (i.e., after 18:00), the backup duration actually reduces as T_D rises. The truth is that an electric vehicle (EV) won't have enough time to recharge after discharging to support the grid if the duration of the power loss is too long. As a result, to ensure full charge before departure, the EV-UPS chooses to provide less backup energy to the grid, resulting in a decrease in backup time, as shown in Figure 13(a). According to Figure 13(b), the load downtime percentage increases as the T_D increases, resulting in lower load reliability. Especially if the T_D is 8 hours, the load downtime percentage is greater than 60%, implying that the load downtime lasts longer than 4.8 hours.

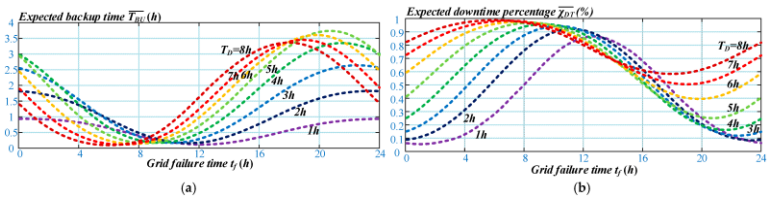

Figure 13: $\overline{\mathrm{T_{BU}}}$ and $\overline{\chi_{\mathrm{DT}}}$ for different power outage durations (a) Expected backup time $\overline{\mathrm{T_{BU}}}$; (b) Expected load downtime percentage $\overline{\chi_{\mathrm{DT}}}$.

The results of $\overline{\chi_{DT}}$ for various T_D can also be plotted in 3D, as shown in Figure 14. The color in the figure represents the value of $\overline{\chi_{DT}}$. According to the graph, as T_D increases, so does the range of the red area. This means that as T_D increases, so does the percentage of load downtime. When T_D is low, the blue area's range is relatively large, indicating that the corresponding load downtime percentage is low and load reliability is high. Furthermore, the red area is closer to the center of the t_f-axis, indicating that the load downtime percentage is higher if the grid failure occurs during the day.

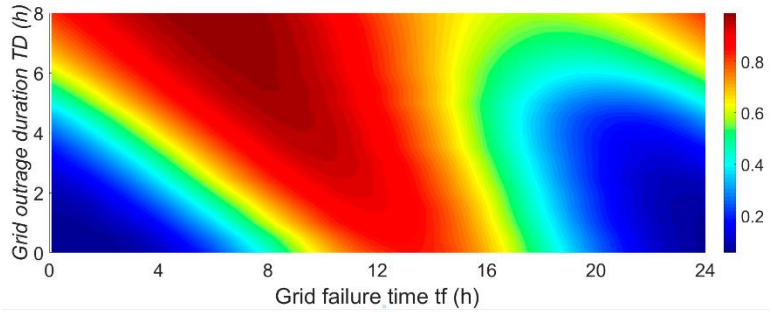

Figure 14: $\overline{\chi_{DT}}$ for different power outage durations.

4.2 Variable Load Condition

Figure 15 depicts a daily typical household load with varying load power over time. Refrigeration, heating and cooling, lighting, cooking, and washing and drying are the most common types of appliances. It should also be noted that the load power after work is relatively high, especially between 18:00 and 22:00. It is worth noting that the peculiarities of a particular household's consumption cyclogram are not taken into account.

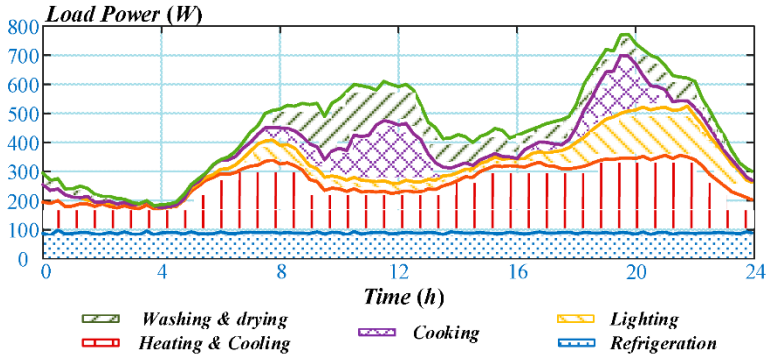

Figure 15: Typical household load.

The results of $\overline{E_{BU}}$ and $\overline{T_{BU}}$ for the typical household load in Figure 15 are obtained using the same method as for the constant load conditions, and are shown in Figure 16. It is worth noting that the grid failure duration is set to one hour. According to Figure 16, when the grid fails during the day, the backup time and energy are both relatively low. When the grid fails during the night, the backup time and energy are relatively long. The backup energy is highest between 18:00 and 22:00, because the load power is high during this time period.

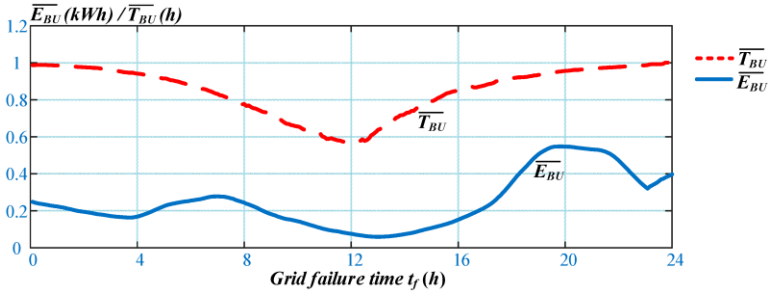

Figure 16: Results of $\overline{E_{BU}}$ and $\overline{T_{BU}}$ for typical household load.

Figure 17 displays the results of $\overline{T_{BU}}$ for various grid outage durations T_D. The color in the graph represents the value of $\overline{T_{BU}}$. Figure 17 shows that as the grid outage duration T_D increases, the color begins to turn yellow, indicating that the backup time $\overline{T_{BU}}$

increases. Also, when the grid fails during the day, the blue color appears more frequently, indicating that the corresponding backup time is short.

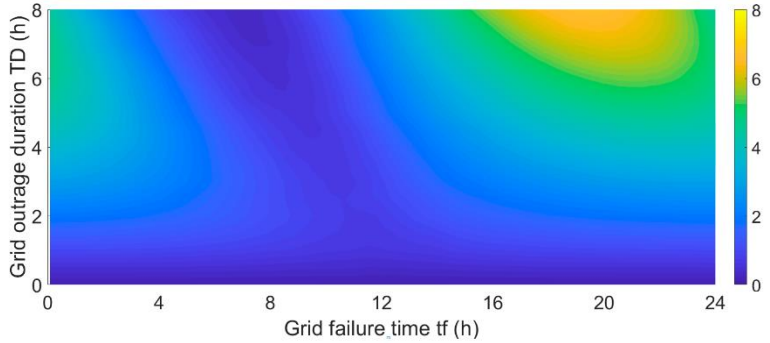

Figure 17: Results of backup time $\overline{T_{BU}}$.

The results of $\overline{\chi_{DT}}$ for various T_D can also be plotted in 3D, as shown in Figure 18. The color in the figure represents the value of $\overline{\chi_{DT}}$. According to the graph, as T_D increases, so does the range of the red area. This means that as T_D increases, so does the percentage of load downtime. When T_D is low, the blue area's range is relatively large, indicating that the corresponding load downtime is low and the load reliability is high.

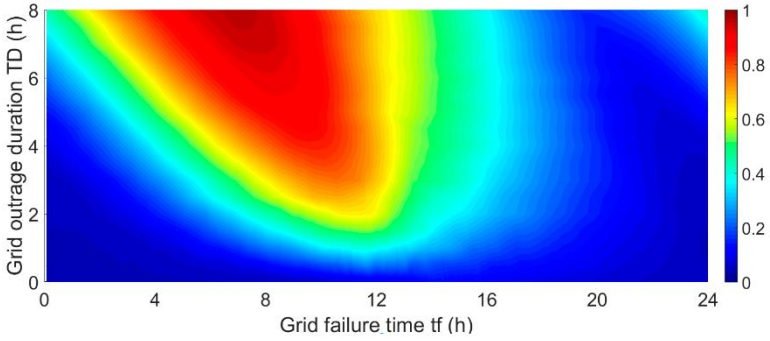

Figure 18: Results of load downtime percentage $\overline{\chi_{DT}}$.

Figure 18 shows that the red area remains large, and thus the load downtime percentage remains high. An improvement

strategy is investigated in the following section to further reduce load downtime and increase load reliability.

5. Improvement of Backup Capacity

5.1 Concept of the Improved Strategy

Figure 19(a) depicts the previous FCBD strategy concept. According to the above analysis, backup capability is relatively low. The main reason is that EVs attempt to be fully charged before departure, limiting the amount of backup energy available. Another disadvantage of the previous strategy is that the duration of the grid outage must be known in advance in order to implement the algorithm. However, the length of a grid outage is difficult to predict in practice.

As a result, an improved strategy is proposed in Figure 19(b). Even when the grid is normal, EVs try to be fully charged before leaving. During the duration of the grid outage, however, the battery energy requirement is modified to maintain only above the minimum energy E_{min} plus the next trip energy requirement E_{trip}. More energy can thus be released during the power outage. Furthermore, the next trip will be unaffected. It should be noted that the value of E_{trip} can make use of the data from the previous trip. Another advantage of this strategy is that the duration of the grid outage is not required by the algorithm.

Furthermore, the load can be reduced during the duration of the grid outage, as shown in Figure 19(c), by only powering the essentials, such as cooking, lighting, and heating and cooling. As a result, during the grid outage, power cannot be used for washing and drying or refrigeration. This way, backup capacity can be increased even further. Here is a solution for implementation. When the power goes out, the control system can automatically turn off the power for the washing, drying, and refrigeration. During a grid outage, power is cut off for washing and drying as well as refrigeration. When the grid recovers, the control system can automatically activate the power breaker for the washing and drying and refrigeration systems.

The block scheme for both strategies is presented in Figure 20.

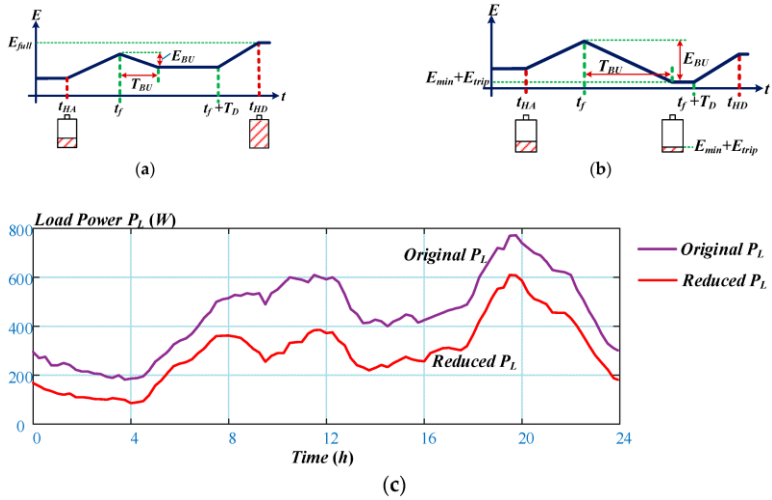

Figure 19: Proposed strategy (a) Previous strategy; (b) Proposed strategy; (c) Load power reduction during grid outage.

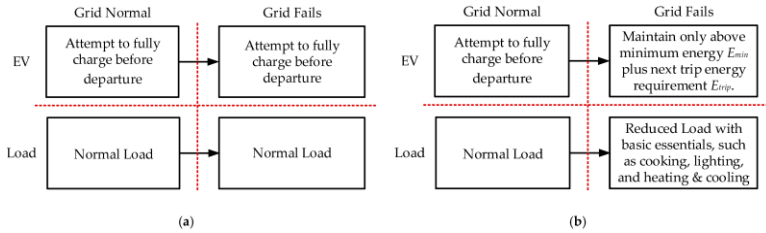

Figure 20: Block scheme for the previous strategy and proposed strategy (a) Previous strategy; (b) Proposed strategy.

5.2 Backup Capacity Calculation

The backup capacity using the improved strategy can be calculated using the same method as in section 2. Similarly, four cases are presented based on various grid failure times t_f (see Figure 5). Using case C as an example, three subcases can be obtained, as shown in Figure 21.

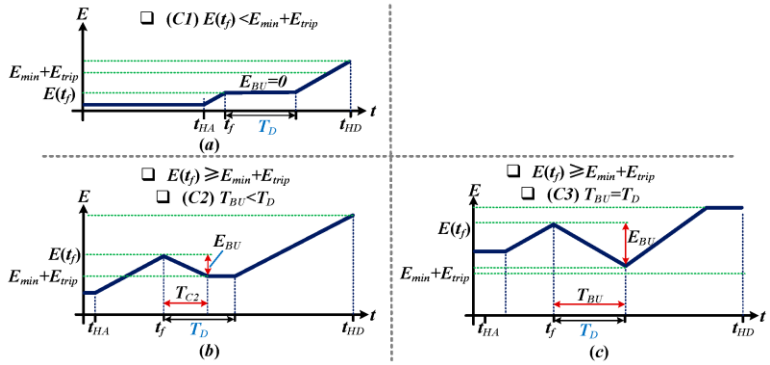

Figure 21: Three sub-cases for case C.

In case *C1*, $E(t_f)$ is less than E_{min} plus E_{trip}. Therefore, the EV cannot release the backup energy. E_{BU} and T_{BU} are both zero in this case as shown in .

$$\begin{cases} E_{BU}(t_f) = 0 \\ T_{BU}(t_f) = 0 \end{cases} \quad (Case\ C1) \tag{16}$$

In cases C2 and C3, $E(t_f)$ equals E_{min} plus E_{trip}, allowing the stored energy to be released for backup. In the case of C2, the stored energy cannot last the entire duration of T_D. As a result, the EV energy reaches its limit in the middle of the T_D. In (17), the backup energy E_{BU} and backup time t_{BU} in case C2 are shown from Figure 21(b).

$$\begin{cases} E_{BU}(t_f) = E(t_f) - (E_{min} + E_{trip}) \\ E_{BU}(t_f) = \int_{t_f}^{t_f+T_{C2}} \frac{P_L(t)}{\eta_{dis}} dt \quad (Case\ C2) \\ T_{BU}(t_f) = T_{C2} \end{cases} \tag{17}$$

In the case of C3, the stored energy can last the entire duration of T_D. As a result, the EV can discharge continuously throughout the T_D. In the case of C3, the backup energy E_{BU} and backup time T_{BU} are expressed as shown in (18).

$$\begin{cases} E_{BU}(t_f) = \int_{t_f}^{t_f+T_D} \frac{P_L(t)}{\eta_{dis}} dt & (Case\ C3) \\ T_{BU}(t_f) = T_D \end{cases} \quad (18)$$

The backup energy E_{BU} and backup time T_{BU} for other cases can be calculated using the same method, which will not be discussed further here.

5.3 Backup Capacity Results

Figure 22 shows the results of the backup time ($\overline{T_{BU}}$) using the previous strategy and the improved strategy, with the grid failure duration set to 8 hours. Figure 22 shows that the improved strategy significantly increases backup time. With the improved strategy, backup time can be increased by two hours when the grid fails during the night. However, if the grid fails during the day, the backup time is nearly identical to that of the old strategy.

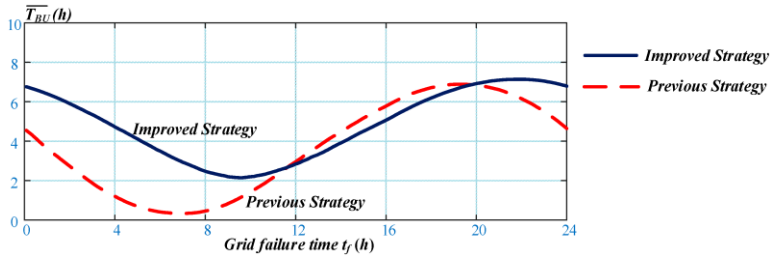

Figure 22: Results of $\overline{T_{BU}}$ with two different strategies.

Figure 23 depicts the results of $\overline{\chi_{DT}}$ for various T_D after using the improved strategy. The color in the figure represents the value of $\overline{\chi_{DT}}$. When compared to the previous strategy's results (see Figure 18), the red area is reduced to yellow. This means that the improved strategy reduces load downtime by approximately 20%. In addition, the improved strategy expands the blue area. As a result of the improved strategy, load downtime is reduced and load reliability is increased.

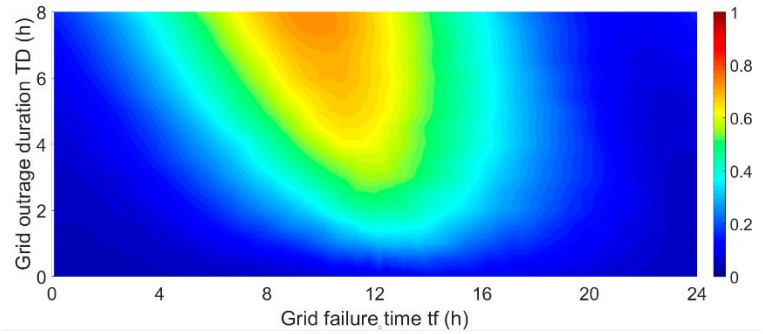

Figure 23: Results of $\overline{\chi_{DT}}$ with the improved strategies.

6. Experimental Verifications

The setup for a 5kW EV-UPS experimental platform is shown in Figure 24(a), where the battery is used to simulate the EV. Figure 24(b) depicts the system's topology as well. Every five minutes, the system's data is sent to users via Ethernet cable.

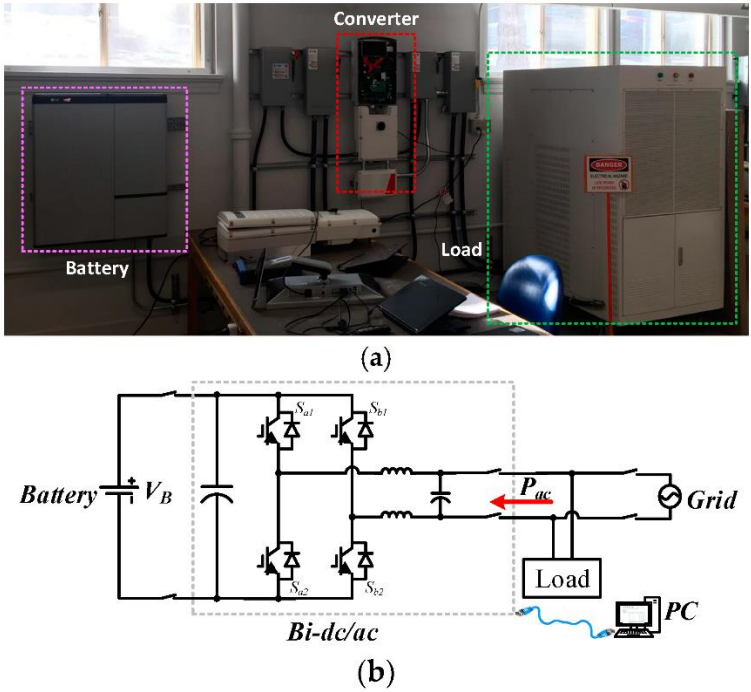

Figure 24: Experimental platform (a) Experimental setup; (b) Topology.

The parameters of the system are presented in Table 2.

Table 2: Parameters of the system.

Item	Value
Battery voltage range	350~450V
Battery capacity	9.8kWh
EV minimum energy E_{min}	0.2×9.8kWh
Maximum input current	17.5A
Charging power	5kW
Nominal grid voltage (L-L)	240V
Nominal grid frequency	50Hz
Maximum continuous ac current	21A @ 240V
Load power	1kW
Home arrive time t_{HA}	18:00h
Home departure time t_{HD}	8:00h
Battery SOC when arriving home	0.85

In the first case, the grid outage lasts three hours. Furthermore, the grid failure is assumed to begin at 5:00 and last until the departure at 8:00. Figures 25 and 26 show the experimental results after using the old strategy and the improved strategy, respectively. It is worth noting that the data is collected every 5 minutes and then plotted using MATLAB. According to the data, when the EV arrives home at 18:00h, the battery begins to charge itself, and the battery is fully charged before the grid goes down. If the old strategy is used (see Figure 25), the battery will be unable to discharge energy in order to ensure full charge before departure. As a result, the backup time is 0 and the load downtime percentage is 100%. If the improved strategy is used, the battery can discharge energy to support the load after the grid fails, and the discharging time can be extended to three hours. As a result, the duration of the grid outage can be fully covered, and the load downtime percent-age is 0%. Furthermore, before departure, the battery SOC is 0.65. As a result, the trip requirement can also be met.

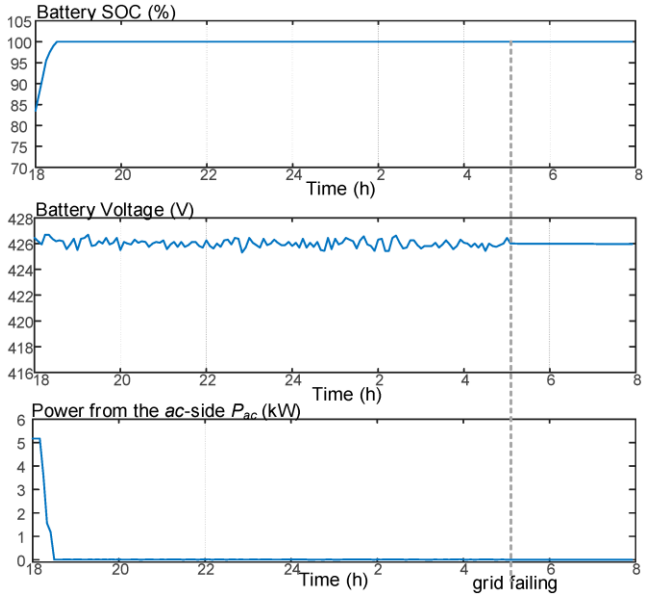

Figure 25: Results using the old strategy (case 1).

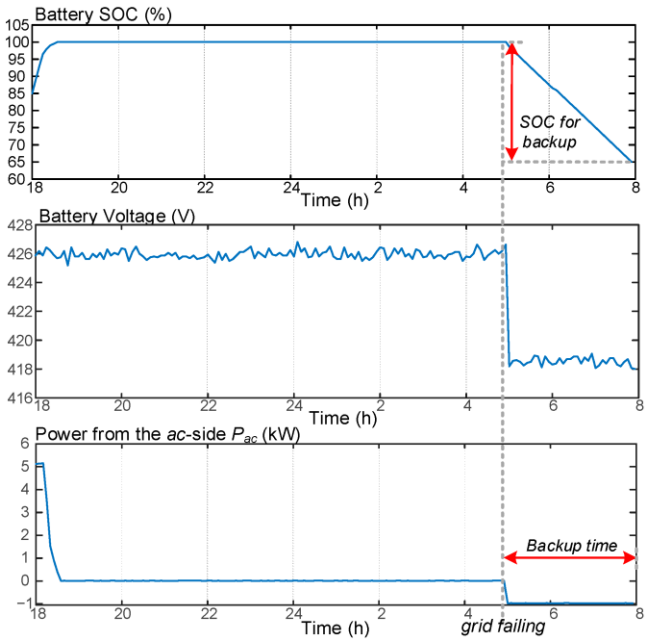

Figure 26: Results using the improved strategy (case 1).

The grid outage duration is set to 5 hours in the second case. It is assumed that the grid failure begins at 2:30 and ends at 7:30. Figures 27 and 28 show the experimental results after using the old strategy and the improved strategy, respectively. According to the data, when the EV arrives home at 18:00h, the battery begins to charge itself, and the battery is fully charged before the grid goes down. The battery can discharge and support the load for 2.5 hours if the old strategy is used (see Figure 27). The full charge can thus be guaranteed prior to departure. As a result, the backup time is 2.5 hours and the load downtime is 50%. If the improved strategy is used, the charging time can be increased to five hours. As a result, the duration of the grid outage can be fully covered, and the load downtime percentage is 0%. Also, before departure, the battery SOC is 0.65, and the trip requirement can be met.

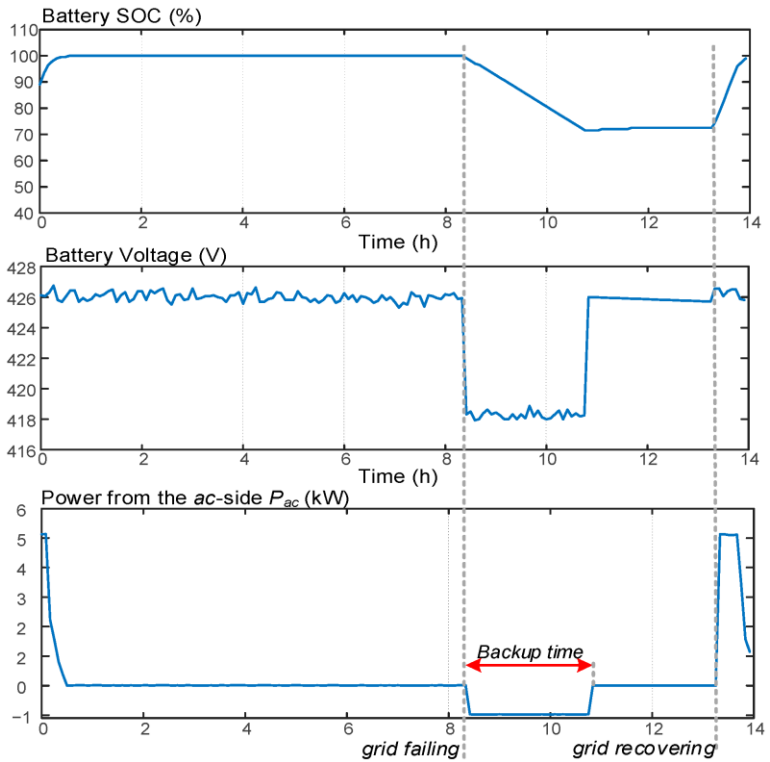

Figure 27: Results using the old strategy (case 2).

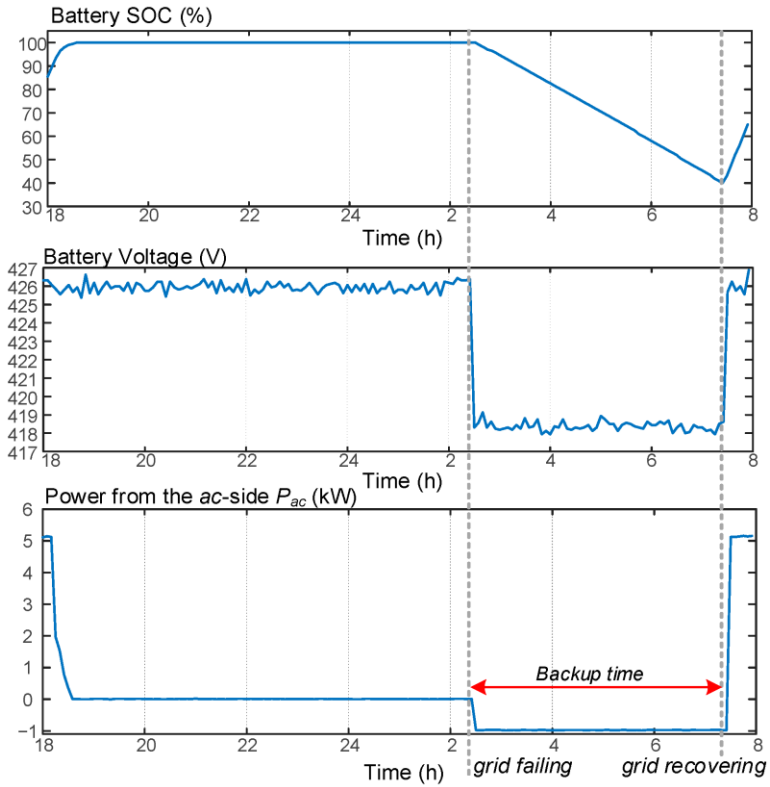

Figure 28: Results using the improved strategy (case 2).

Figure 29 depicts the backup time results for the two preceding cases. It can be seen that the improved strategy significantly increases backup time.

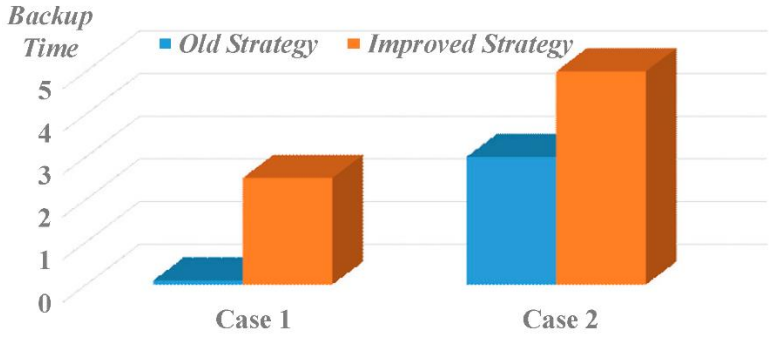

Figure 29: The results of the backup time for the above two cases

7. Conclusion

The use of EVs as UPSs for households, particularly in rural areas, can greatly improve the reliability of household power. The UPS architectures for single- and multiple-EV are presented first. The methodology for calculating backup capacity for EV-UPS systems is then presented based on the EV mobility pattern, and four cases based on different grid failure times are detailed. According to the calculations, if the grid fails during charging, the EV-UPS can completely cover the outage. A Monte Carlo simulation is also run to account for the uncertainty of the daily travel parameters. The duration of the power outage is also considered. The percentage of load downtime increases with the duration of the power outage, resulting in lower load reliability. An improved strategy is proposed to increase backup capacity even further. The battery energy requirement is changed during the grid outage to maintain only above the minimum energy E_{min} plus the next trip energy requirement E_{trip}. More energy can thus be released during the power outage. Furthermore, the next trip will be unaffected. Furthermore, during a grid outage, the load can be reduced by only using power for the essentials. In the case study, the improved strategy can increase backup time by two hours. Finally, a 5kW EV-UPS testing platform is constructed. The experimental results show that the improved strategy significantly improves backup time.

References

1. F. Musavi, W Eberle. Overview of wireless power transfer technologies for electric vehicle battery charging. IET Power Electronics. 2014; 7: 60-66.
2. E Sortomme, MA El-Sharkawi. Optimal scheduling of vehicle-to-grid energy and ancillary services. IEEE Transaction on Smart Grid. 2012; 3: 351-359.
3. C Liu, KT Chau, D Wu, S Gao. Opportunities and Challenges of Vehicle-to-Home, Vehicle-to-Vehicle, and Vehicle-to-Grid Technologies. Proceedings of the IEEE. 2013; 101: 2409-2427.

4. DT Nguyen., LB Le. Joint optimization of electric vehicle and home energy scheduling considering user comfort preference. IEEE Trans. Smart Grid. 2014; 5: 188–199.
5. MHK Tushar, C Assi, M Maier, MF Uddin. Smart microgrids: Optimal joint scheduling for electric vehicles and home appliances. IEEE Trans. Smart Grid. 2014; 5: 239–250.
6. V Monteiro et al., On-board electric vehicle battery charger with enhanced V2H operation mode. Proc. IEEE Ind. Electron. Conf. (IECON), Dallas, TX, USA. 2014; 1636–1642.
7. 'Power failures far more common in remote parts of B.C.', http://www.vancouversun.com/technology/Power+failures+more+common+remote+parts/11311997/story.html
8. W Zhang, K Spence, R Shao, L Chang. Optimal Scheduling of Spinning Reserve and User Cost in Vehicle-to-Grid (V2G) Systems. 2018 IEEE Energy Conversion Congress and Exposition (ECCE), Portland, Oregon. 2018.
9. SB Bekiarov, A Emadi. Uninterruptible power supplies: classification, operation, dynamics, and control. APEC. Seventeenth Annual IEEE Applied Power Electronics Conference and Exposition, Dallas, TX, USA. 2002; 1: 597-604.
10. SS Williamson. AK Rathore, F Musavi. Industrial Electronics for Electric Transportation: Current State-of-the-Art and Future Challenges. IEEE Transactions on Industrial Electronics. 2015; 62: 3021-3032.
11. Z Zhao, Q Xu, Y Dai, A Luo. Minimum resonant capacitor design of high-power LLC resonant converter for comprehensive efficiency improvement in battery charging application. IET Power Electronics.2018; 11: 1866-1874.
12. V Monteiro, B Exposto, JC Ferreira, JL Afonso. Improved Vehicle-to-Home (iV2H) Operation Mode: Experimental Analysis of the Electric Vehicle as Off-Line UPS. IEEE Transactions on Smart Grid. 2017; 8: 2702-2711.
13. W Zhang et al., Seamless Transfer Control Strategy for Fuel Cell Uninterruptible Power Supply System. IEEE Transactions on Power Electronics. 2013; 28: 717-729.
14. R Yu, W Zhong, S Xie, C Yuen, S Gjessing, et al. Balancing Power Demand Through EV Mobility in Vehicle-to-Grid

Mobile Energy Networks. IEEE Transactions on Industrial Informatics. 2016; 12: 79-90.
15. W Zhang, C Dreise, R Shao, L Chang. An improved minimum-cost charging schedule for large-scale penetration of electric vehicles," 2018 IEEE Applied Power Electronics Conference and Exposition (APEC), San Antonio, TX. 2018; 3411-3417.
16. M Yilmaz, PT Krein. Review of Battery Charger Topologies, Charging Power Levels, and Infrastructure for Plug-In Electric and Hybrid Vehicles. IEEE Transactions on Power Electronics. 2013; 28, 2151-2169.
17. Haider, Zunaib Maqsood et al. Optimal Management of a Distribution Feeder During Contingency and Overload Conditions by Harnessing the Flexibility of Smart Loads. IEEE Access. 2021; 9: 40124-40139.
18. Jaruwatanachai, Pramote, Yod Sukamongkol, Taweesak Samanchuen. Predicting and Managing EV Charging Demand on Electrical Grids: A Simulation-Based Approach. Energies. 2023; 16: 35-62.
19. Singh, Balvender, Adam Slowik, Shree Krishan Bishnoi, Mandeep Sharma. Frequency Regulation Strategy of Two-Area Microgrid System with Electric Vehicle Support Using Novel Fuzzy-Based Dual-Stage Controller and Modified Dragonfly Algorithm. Energies. 2023; 16: 3407.